Published in final edited form as:
Anal Chem. 2006 July 15; 78(14): 5134–5142. doi:10.1021/ac060525v.

A Detailed Map of Oxidative Post-translational Modifications of Human p21ras sing Fourier Transform Mass Spectrometry

Cheng Zhao[1,2], **Mahadevan Sethuraman**[2], **Nicolas Clavreul**[3], **Parminder Kaur**[1,2], **Richard A. Cohen**[2,3], and **Peter B. O'Connor**[1,2]

[1]Mass Spectrometry Resource, Department of Biochemistry, Boston University School of Medicine, Boston, Massachusetts 02118

[2]Cardiovascular Proteomics Center, Boston University School of Medicine, Boston, Massachusetts 02118

[3]Vascular Biology Unit, Boston University School of Medicine, Boston, Massachusetts 02118

Abstract

P21ras, the translation product of the most commonly mutated oncogene, is a small guanine nucleotide exchange protein. Oxidant-induced post-translational modifications of p21ras including *S*-nitrosation and *S*-glutathiolation have been demonstrated to modulate its activity. Structural characterization of this protein is critical to further understanding of the biological functions of p21ras. In this study, high resolution and high mass accuracy Fourier Transform Mass Spectrometry (FTMS) was utilized to map, in detail, the post-translational modifications of p21ras (H-ras) exposed to oxidants by combining bottom-up and top-down techniques. For peroxynitrite-treated p21ras, five oxidized methionines, five nitrated tyrosines, and at least two oxidized cysteines (including C118) were identified by "bottom-up" analysis and the major oxidative modification of C118, Cys^{118}-SO_3H, was confirmed by several tandem mass spectrometry experiments. Additionally, "top-down" analysis was conducted on p21ras *S*-glutathiolated by oxidized glutathione and identified C118 as the major site of glutathiolation among the four surface cysteines. The present study provides a paradigm for an effective and efficient method not only for mapping post-translational modifications of proteins but also for predicting the relative selectivity and specificity of oxidative post-translational modifications especially using top-down analysis.

Introduction

The human p21ras (Ras) family consists of three frequently mutated proto-oncogenes, H-ras, K-ras, and N-ras, which encode ~21 kDa protein products.1, 2 The Ras proteins are small guanine nucleotide exchange proteins that play a critical role as signal transducers in the regulation of a number of cellular processes, including cell growth, differentiation, and apoptosis.1, 3 They cycle between inactive GDP-bound state and active GTP-bound state regulated by guanine nucleotide exchange factors (GEFs) and GTPase-activating proteins (GAPs).4–6 These regulatory proteins bind to Ras and regulate the exchange of GDP with GTP. Ras can be modified and activated by reactive nitrogen species (RNS) including nitric oxide (·NO), nitrogen dioxide ($\cdot NO_2$), dinitrogen trioxide (N_2O_3), and peroxynitrite 7 as well as reactive oxygen species (ROS) such as superoxide anion radical ($O_2^{-}\cdot$) and hydrogen peroxide (H_2O_2).8–15 ·NO is the best characterized redox modulator of Ras activity as it has

Correspondence to: Peter B. O'Connor.

been shown to promote Ras GDP dissociation in *vitro*, GTP binding to Ras in *vivo*, and stimulation of signaling pathways downstream of Ras.[16–22]

Peroxynitrite anion ($ONOO^-$), the product of the reaction between superoxide anion ($O_2^{-}\cdot$) and nitric oxide (·NO),[23, 24] is a potent oxidant formed in endothelial cells[25, 26] which oxidizes a wide range of biological targets.[23, 27, 28] Ras activity is potentially modulated by reversible as well as irreversible oxidative post-translational modifications. *S*-oxidation and *S*-nitrosation of Ras by peroxynitrite have been demonstrated *in vitro* and *in vivo*.[13–15, 29] In particular, four surface cysteines (C118, C181, C184 and C186) with reactive thiol groups can regulate H-ras activity in response to oxidative modifications. The reaction of ROS/RNS with Cys-118, which is located in the Ras guanine nucleotide-binding motif (NKCD motif),[30, 31] has been implicated in activation of Ras leading to downstream signaling to Raf-1/Mek/Erk to mediate cellular responses.[7, 13, 32, 33] The role of oxidative modifications of the three terminal cysteines is unclear, but because they are involved in membrane localization of the protein,[34–36] they could regulate the activation of Ras.

Glutathione (GSH), a tripeptide γ-glutamyl cysteinyl glycine, is oxidized by ROS/RNS to glutathione disulfide, GSSG. In mammalian cells GSH is the most abundant low molecular weight thiol, and thus it frequently binds to protein thiols to form mixed disulfides, a process termed *S*-glutathiolation. *S*-glutathiolated Ras (GSS-Ras) has been suggested to take part in cellular regulation.[7, 12, 13]

It has been generally accepted that *S*-oxidation, *S*-nitrosation, and *S*-glutathiolation of Ras is involved in cell signaling,[37, 38] but the relative importance by which these modifications directly regulate activity remains poorly understood. The role of *S*-nitrosation of Ras C118 in mediating guanine nucleotide exchange and that of farnesylation of C186 and palmitoylation of C181 and C184 in mediating membrane localization has recently been studied by heteronuclear NMR and triple quadrupole mass spectrometry.[39–41] However, the reports of structural characterization of post-translational modifications on full-length Ras protein are somewhat limited.[41]

Post-translational modification (PTM) mapping of biological samples is not only chemically and biologically challenging, but also technically demanding, particularly because some modifications may be at very low abundance and others are labile. The development of electrospray ionization (ESI)[42] and matrix-assisted laser desorption ionization (MALDI)[43, 44] techniques provide the soft ionization methods needed for mass spectrometric analysis of nonvolatile protein and peptide molecules. These two techniques, when combined with Fourier Transform mass spectrometry (FTMS), provide ideal instrumentation for structural analysis of PTMs due to superior resolving power and mass accuracy. Furthermore, FTMS is highly flexible with MS/MS experiments that utilize a variety of fragmentation techniques such as collision activated dissociation (CAD),[45] multiple storage-assisted dissociation (MSAD),[46, 47] infrared multiphoton dissociation (IRMPD),[48] sustained off-resonance irradiation collision activation dissociation (SORI-CAD)[49, 50] and electron-capture dissociation (ECD).[51–53] In particular, ECD directs fragmentation to the peptide backbone and allows labile modifications to remain attached during the fragmentation process.[54–57] In addition, a qQq front end has been combined with the ICR cell in FTMS.[58, 59] In this hybrid design ions can be isolated in Q1 with separation windows less than 1 *m/z* unit[59] which improves analysis of complex mixtures since the precursor ions can be isolated without HPLC separation. Another advantage of this design is that a low abundance ion after Q1 isolation can be accumulated for a longer time in Q2 to increase the quantity of that ion for better MS/MS spectra.

The high resolution and high accuracy of FTMS make "top-down analysis",[60, 61] a relative new technology, possible. In top-down analysis, the intact protein is directly fragmented without enzymatic digestion. Compared to the traditional "bottom-up analysis", which involves enzymatic digestion first and then MS/MS analysis of the resulting peptides, the top-down analysis, by definition, achieves 100% sequence coverage and does not miss post-translational modifications. However, the number of inter-residue bond cleavages generated by doing top-down analysis varies with the efficiency of fragmentation, so that multiple sequence changes resulting in unchanged mass would not be detected unless there are cleavages between those modifications. Although it is highly demanding of instrumentation and sample preparation techniques and the resulting data are far more complex and difficult to analyze, top-down analysis is, without doubt, a valuable complementary technique to bottom-up analysis.

This study was focused on structural characterization of oxidant-induced post-translational modifications on p21ras using combined bottom-up and top-down techniques in order to generate a complete map of the post-translational modifications of p21ras. The oxidative modifications observed, including some very low abundance modifications of peroxynitrite-treated p21ras, were mapped in detail by bottom-up analysis and several modifications on Cys-118 were confirmed by CAD and ECD MS/MS fragmentation. Also, the number of glutathiolated cysteines in p21ras treated with oxidized glutathione disulfide (GSSG) was determined by the intact mass difference between glutathiolated p21ras and the control sample, and the major site of *S*-glutathiolation was identified by top-down analysis. This structural information will aid in understanding the function of p21ras.

Methods

Materials

Recombinant *p21ras* was obtained in buffer containing 20 mM Tris (pH 8.0), 45 mM NaCl, 5 mM $MgCl_2$, 1 mM dithiothreitol (DTT) and 50% glycerol from BIOMOL (Plymouth Meeting, PA) and peroxynitrite was obtained from Calbiochem (San Diego, CA). GSSG and all chemicals were purchased from Sigma Chemical Co. (St. Louis, MO). Trypsin was purchased from Promega (Madison, WI).

Sample preparation

Recombinant *p21ras* (10–20 μg) was dialyzed to remove commercial buffers components and treated for 5 min at 37°C with peroxynitrite ($ONOO^-$, 100–250 μM) or with GSSG (100 μM) in phosphate buffer (0.1 M, pH 7.0). The control and treated samples were dialyzed against 100 mM ammonium bicarbonate buffer before used for FTMS experiments. For "bottom-up" analysis, the control and the modified samples were digested with trypsin at 1:25 (w/w) in 100 mM ammonium bicarbonate (pH 8.0) for 3 h at 37°C and purified with Poros 50 R1 solid phase extraction material (Applied Biosystems, Foster City, CA). For "top-down" analysis, the control and the modified samples were purified with Poros 50 R1 material.

FTMS instrumentation

A custom built qQq-FTMS with a nanospray source and 7T actively shielded magnet (Cryomagnetics Inc., Oak Ridge, TN) was utilized in this study.[58, 59] The "qQq front-end" refers to a focusing rf-only quadrupole (Q0), followed by a resolving quadrupole (Q1), and a LINAC quadrupole collision cell (Q2).[62, 63] Ions can be isolated in the mass resolving Q1 and accumulated in Q2 prior to analysis in the ICR cell. The instrument was designed to employ several fragmentation methods, including nozzle-skimmer fragmentation, Q2 collisionally activated dissociation (Q2 CAD),[45] Multipole Storage Assisted Dissociation

(MSAD),46, 47 electron capture dissociation (ECD),51–53 infrared multiphoton dissociation (IRMPD),48 and sustained off-resonance irradiation (SORI) CAD.49, 50, 64 The front-end quadrupoles were controlled using the program LC2Tune 1.5 (MDS Sciex, South San Francisco, CA), and the program IonSpec99 (IonSpec, Lake Forest, California) controlled data acquisition in the ion cyclotron-resonance (ICR) cell. The purified and dried samples were dissolved in 50/50 acetonitrile/water containing 1% formic acid for the peptide samples and 0.1% trifluoroacetic acid for the protein samples to a concentration of ~1 pmol/μl solution. A ~2–3 μl sample was loaded into a glass capillary tip pulled with a micropipette puller (Model P-97, Sutter Instruments Co., Novato, CA) to ~1 μm orifice diameter and a stainless steel wire was inserted into the distal end of the tip to form the electrical connection. For CAD experiments, the parent ions were isolated by Q1, and were fragmented by low energy (15–30 eV) collisions with N_2 gas in Q2. For ECD experiments, the parent ions were isolated in Q1 and externally accumulated in Q2. After being transmitted and trapped into the cylindrical ICR cell, ions were irradiated with ~0.2 eV electrons from a 1.2 A heated dispenser cathode65 for 15 to 300 ms and were fragmented. The total pulse duration for CAD and ECD experiments varied between 1000 ms and 2 s and all data were analyzed without apodization and with two zero-fills to improve mass accuracy. The standard ICR conditions used in this study were as same as those in prior publications.58, 59

Results and discussion

Unmodified p21ras

Figure 1A (left) shows the ESI spectrum of a sample of intact purified p21ras prepared in the presence of DTT. The resolved isotopic distributions of several high abundance peaks were fitted to model distribution (dots),66 the monoisotopic molecular weight (MI) of this sample was determined to be 21284.4032 Da, which is consistent with the theoretical mass of intact p21ras, 21284.5511 Da. This 7 ppm difference is within the expected error range of ~5–10 ppm for externally calibrated FTMS data. When comparing the mass of intact p21ras protein prepared in the absence (Figure 1B), or in the presence of DTT (Figure 1A (left)), a 2 Da mass difference was detected, suggesting the presence of a disulfide bond. Because the p21ras sample was purchased in buffer containing DTT, this disulfide bond probably re-formed after removal of the DTT by dialysis.

In order to localize this disulfide bond, these two samples were digested using trypsin. A peptide spanning amino acids 170–185 including Cys 181 and Cys 184 was identified in both samples which was 2 Da lighter in the sample without DTT (Figure 2A, left) than in the sample treated with DTT (Figure 2A, right). Q2 CAD MS allowed localization of a disulfide bond to the two cysteines of the peptide (Figure 2B). This is the first report of a disulfide bond between C181 and C184 p21ras. However, since the p21ras used in this study was recombinant protein expressed in bacteria and C181 and C184 were not palmitoylated, this disulfide bond may not exist in intracellular situation.

Peroxynsitrite (PN) treated p21ras

The Ras sequence suggests that oxidative modifications could happen on many different sites such as methionines, cysteines, and tyrosines. The ESI spectrum of the intact purified p21ras treated with a 10-fold excess peroxynitrite is shown in Figure 1A (right). Due to the complex and heterogeneous oxidative modifications on p21ras, the spectrum still yielded a signal to noise ratio < 5 even after several steps of sample cleaning. The isotopic distribution of individual charge states cannot be resolved (inset), and apparently includes several overlapping distributions. The top-down method is very difficult under such conditions. Nozzle skimmer fragmentation was applied to all the charge states, but the data were too

complicated to analyze. Thus, the bottom-up method was utilized to map the oxidative post-translational modifications on this sample. Fortunately, 100% sequence coverage was obtained, and Figure 3 shows the spectrum of the tryptic digest mixture. The peaks were labeled with the peptides positions. Those labeled with * indicate methionine oxidation modification, those labeled with $^{\Delta}$ indicate both methionine oxidation and cysteine sulfonic modification, and those labeled with $^{\circ}$ indicate nitration on the peptides. The sequences of two peptides (6–16 and 17–42) (insets) were confirmed by CAD MS/MS data, and they were then utilized for internal calibration of the rest of the spectrum. Table 1 lists all the detected peaks after internal calibration. Most of the errors between experimental and theoretical mass of these peptides are within 2 ppm except several between 2 ppm and 3 ppm for peptides below ~S/N = 5. Overall, the average of the absolute value of the error in these peptides is 1.09 ±0.74 ppm.

Figure 4A plots the modifications detected in peroxynitrite-treated p21ras including irreversible methionine, tyrosine, and cysteine oxidations.67–72 Five methionines (M1, M67, M72, M111, M182) were oxidized and five tyrosines (Y4, Y40, Y96, Y137, Y157) were nitrated. Cys118, which resides in the “NKCD” loop, the GTP binding site, was oxidized. Cys118 sulfenic acid (SOH), sulfinic acid (SO_2H), sulfonic acid (SO_3H), and S-nitrosothiol (SNO) were all observed (Figure 5A) though those with sulfenic acid, sulfinic acid and nitrosothiol modifications were very low abundance. One possible reason for the low abundance *S*-nitrosation is that the nitrosothiol can be further oxidized to sulfonic acid.73 At least one of the three terminal cysteines (Cys 181, Cys184, and Cys186) was oxidized into Cys-SO_3H. Peaks corresponding to two and three terminal cysteines with sulfonic modifications were also detected, but they were much lower intensity than the one with only one sulfonic modification. The abundances of the two primary oxidation products of the peptide 103–123 are shown in Figure 5A. Peptide 103–123 with a single oxidation is clearly the most intense. This peptide could be oxidized either at cysteine or methionine, but the CAD MS/MS data in Figure 5B confirmed that it is oxidized at Met 111, consistent with the higher rate of methionine oxidation over cysteine oxidation. Among the peaks of the peptide 103–123 with both methionine and cysteine modifications (Figure 5A and inset), the one at *m/z* 770.3 representing the peptide with both methionine oxidation and cysteine sulfonic oxidation is the strongest, consistent with either the higher rate of formation or the greater stability of sulfonic acid compared with sulfenic or sulfinic acid. This peak (*m/z* 770.3) was isolated by Q1 and fragmented in Q2 by low energy (15–30 eV) CAD (Figure 5C) as well as in the ICR cell by ECD (Figure 5D). Substantially better cleavage and coverage was observed in the ECD experiment than in the CAD experiment. The results are tabulated in table 2. Multiple b, y ($b_{17–20}$ and $y_{14, 15, 19}$ from CAD) and c, z ($c_{17–20}$ and $z_{15–18}$ from ECD) ions including both Met^{111} oxidation and Cys^{118} sulfonic modification were detected, and these ions demonstrated that the cysteine and methionine oxidative modifications can survive low energy CAD and ECD conditions. Interestingly, the CAD spectrum (Figure 5C) showed no evidence of sulfate loss, even though sequence coverage was extensive. In the ECD spectrum, both c ($c_{9–20}$) and z ($z_{13, 15–18}$) ions, which contain methionine, show adjacent oxygen-loss (at -15.9949 Da) peaks, indicating that oxidative modification on methionine can be lost under odd electron ECD conditions. Guan, etc.71 studied CAD and ECD of several Met (O)-containing peptides and they reported a characteristic methanesulfenic acid side chain lost (CH_3SOH, 64Da) in CAD, which was also detected in our study.

S-Glutathiolated p21ras

Figure 6A shows the ESI spectrum of intact glutathiolated p21ras which shows at least three groups of charge state distributions. Compared to the ESI spectrum of unmodified p21ras in Figure 1B, the most intense charge state distribution, whose monoisotopic molecular weight

(MI) was 21257.4387 Da (+18 charge state), indicated one glutathione addition to the p21ras and the other two indicated two and three glutathione additions, respectively. For the triply glutathiolated p21ras, the disulfide bond at Cys 181- Cys-184 was cleaved ($MI_{p21ras\ +3SG} - MI_{p21ras\ +2SG} = MI_{SG} + 2Da$).

For the bottom-up experiments on tryptic peptides, all the cysteines, including the terminal three cysteines were glutathiolated (Figure 4B), although it is possible that some of them were formed by exchange of disulfide bonds between GSSG and p21ras protein/tryptic peptides during sample digestion. Although with bottom-up data, it is impossible to determine which cysteine is the major site of glutathiolation on p21ras, this difficulty is solved with top-down analysis, in which the specific intact modified protein ions can be selectively isolated and fragmented. The major glutathiolated p21ras ion (Figure 6A) was isolated by Q1 and then directly fragmented in Q2 by CAD and in the ICR cell by ECD and the resulting spectra are shown in Figure 6B and Figure 6C. Although only 64 of 188 inter-residue bonds were cleaved, the fragment ions provided enough information to localize the modification. The CAD spectrum in Figure 6B did not show any glutathiolation on the b_{112} fragment ion but b_{131} did include one glutathiolation indicating that a cysteine between amino acid 112 and 131 from the N-terminus was involved. Similarly, the ECD spectrum in Figure 6C, showed no glutathiolation at z_{38} but showed one at z_{79}, indicating that the glutathiolation was on a cysteine between amino acid 38 and 76 from the C-terminus, thus identifying the site as C118. Therefore, these data identify C118 as the site of most abundant glutathiolation in GSSG-treated p21ras. Thirty-two cleavages ($b_{6–9}$, $b_{18–20}$, $b_{29–31}$, b_{47}, $b_{51–55}$, b_{109}, b_{112}, b_{131}, b_{137}, b_{177}, y_{31}, y_{123}, y_{126}, y_{129}, $y_{131–133}$, $y_{135–136}$, y_{179}, y_{187}) were obtained in CAD top-down analysis, 46 cleavages ($c_{4–9}$, $c_{11–27}$, $c_{29–35}$, $c_{37–38}$, c_{41}, c_{46}, c_{57}, $c_{68–69}$, $c_{83–84}$, c_{87}, $z_{5–6}$, $z_{11–12}$, z_{38}, z_{76}) were obtained in ECD top-down analysis, and 4 complementary pairs (b_{53} and y_{136}, b_{54} and y_{135}, c_{57} and y_{132}, b_{177} and z_{12}) were obtained, resulting in 100% sequence coverage on the singly glutathiolated p21ras. Also, the consecutive sequence tags such as $c_{11–27}$ and $c_{29–35}$ with ~2 ppm mass accuracy is more than sufficient to accurately assign the protein identity.

In order to further analyze Cys^{118}-SSG, the 103–123 peptide with glutathiolated C118 was isolated by Q1 from the digestion mixture and fragmented using low energy (15–25 eV) CAD and a ECD MS/MS experiments (Figure 7A and B). $C_{17–20}$, z_8, $z_{11–13}$, $z_{15–19}$ and $y_{6–12}$, $y_{14–20}$ including Cys^{118}-SSG were detected, confirming this modification. As before, the ECD experiment provided higher cleavage coverage than the CAD experiment, and most of the errors between experimental and theoretical mass of b, y and c, z ions were within 2 ppm (Table 3). During the ECD experiment, two glutathione losses were detected on z ions (z_7-SG and z_9-SG) while nine glutathiolated z ions (z_8, $z_{11–13}$, $z_{15–19}$) were observed. The detailed results of these studies are plotted in Figure 4.

Conclusions

This study combined bottom-up and top-down mass spectrometry methods on a recently developed FTMS instrument to study the post-translational modifications on the p21ras. Peroxynitrite-treated p21ras included multiple complex modifications that, despite their complexity, were analyzed using a bottom up MS/MS approach. Many oxidative modifications and some low abundance modifications such as Cys^{118}-SNO, Cys^{118}-SOH and 0nCys^{118}-SO_2H were identified. It is notable that the SNO modification was stable throughout digestion and MS analysis. Five oxidized methionines, five nitrated tyrosines, and at least two oxidized cysteines, including Cys-118 and one of the terminal cysteines, were identified. The structure of the most abundant oxidative modification on Cys-118, Cys^{118}-SO_3H, was confirmed by low energy CAD and ECD MS/MS experiments. Also, from top-down analysis, Cys-118 is identified as the major glutathiolated cysteine on

p21ras. This top-down analysis was selectively performed on the specific singly glutathiolated p21ras using both CAD and ECD fragmentation, and the peptide 103–123 with the Cys^{118}-SSG modification was isolated from the digests and fragmented to confirm this modification.

The detected mass accuracy of this FTMS instrument on either peptides or fragmentation ions is ~ 2 ppm with internal calibration except for some very weak peaks (signal/noise < 5) for which accuracy suffers due to noise distortion of the peak shapes. This high mass accuracy helps for both protein and peptide identification. In addition, this study provides a paradigm for an effective and efficient method for mapping the post-translational modifications of proteins. With appropriate software and search engines, this method also can be used to identify unknown proteins and peptides.

Supplementary Material

Refer to Web version on PubMed Central for supplementary material.

Acknowledgments

The authors would like to thank Jason J. Cournoyer, Vera Ivleva and Dr. Cheng Lin for the valuable suggestions. This research was supported by NIH P41-RR10888, N01-HV28178, R01 AG27080, P01 HL HL81587, MDS Sciex, the ACS Petroleum Research Fund, and an NIH Post-doctoral Research Fellowship T32 HL07224.

References

1. Campbell SL, Khosravi-Far R, Rossman KL, Clark GJ, Der CJ. Increasing complexity of Ras signaling. Oncogene. 1998; 17:1395–1413. [PubMed: 9779987]
2. Bos JL. Ras Oncogenes in Human Cancer - a Review. Cancer Res. 1989; 49:4682–4689. [PubMed: 2547513]
3. Shields JM, Pruitt K, McFall A, Shaub A, Der CJ. Understanding Ras: 'it ain't over 'til it's over'. Trends in Cell Biol. 2000; 10:147–154. [PubMed: 10740269]
4. Boriack-Sjodin PA, Margarit SM, Bar-Sagi D, Kuriyan J. The structural basis of the activation of Ras by Sos. Nature. 1998; 394:337–343. [PubMed: 9690470]
5. Vetter IR, Wittinghofer A. Signal transduction - The guanine nucleotide-binding switch in three dimensions. Science. 2001; 294:1299–1304. [PubMed: 11701921]
6. Scheffzek K, Ahmadian MR, Kabsch W, Wiesmuller L, Lautwein A, Schmitz F, Wittinghofer A. The Ras-RasGAP complex: Structural basis for GTPase activation and its loss in oncogenic Ras mutants. Science. 1997; 277:333–338. [PubMed: 9219684]
7. Clavreul N, Adachi T, Pimental DR, Ido Y, Schoneich C, Cohen RA. S-glutathiolation by peroxynitrite of p21ras at cysteine-118 mediates its direct activation and downstream signaling in endothelial cells. FASEB Journal. 2006 online January 13, 2006.
8. Stamler JS, Lamas S, Fang FC. Nitrosylation: The prototypic redox-based signaling mechanism. Cell. 2001; 106:675–683. [PubMed: 11572774]
9. Jaffrey SR, Erdjument-Bromage H, Ferris CD, Tempst P, Snyder SH. Protein S-nitrosylation: a physiological signal for neuronal nitric oxide. Nat. Cell Biol. 2001; 3:193–197. [PubMed: 11175752]
10. Eu JP, Sun JH, Xu L, Stamler JS, Meissner G. The skeletal muscle calcium release channel: Coupled O-2 sensor and NO signaling functions. Cell. 2000; 102:499–509. [PubMed: 10966111]
11. Sun J, Xin C, Eu JP, Stamler JS, Meissner G. Cysteine-3635 is responsible for skeletal muscle ryanodine receptor modulation by NO. Proc. Natl. Acad. Sci. USA. 2001; 98:11158–11162. [PubMed: 11562475]
12. Klatt P, Lamas S. Regulation of protein function by S-glutathiolation in response to oxidative and nitrosative stress. Eur. J. Biochem. 2000; 267:4928–4944. [PubMed: 10931175]

13. Adachi T, Pimentel DR, Heibeck T, Hou XY, Lee YJ, Jiang BB, Ido Y, Cohen RA. S-glutathiolation of Ras mediates redox-sensitive signaling by angiotensin II in vascular smooth muscle cells. J. Biol. Chem. 2004; 279:29857–29862. [PubMed: 15123696]
14. Heo JY, Campbell SL. Mechanism of p21(Ras) S-nitrosylation and kinetics of nitric oxide-mediated guanine nucleotide exchange. Biochemistry. 2004; 43:2314–2322. [PubMed: 14979728]
15. Mallis RJ, Buss JE, Thomas JA. Oxidative modification of H-ras: S-thiolation and S-nitrosylation of reactive cysteines. Biochem. J. 2001; 355:145–153. [PubMed: 11256959]
16. Baker TL, Booden MA, Buss JE. S-nitrosocysteine increases palmitate turnover on Ha-Ras in NIH 3T3 cells. J. Biol. Chem. 2000; 275:22037–22047. [PubMed: 10801823]
17. Dawson TM, Sasaki M, Gonzalez-Zulueta M, Dawson VL. Regulation of neuronal nitric oxide synthase and identification of novel nitric oxide signaling pathways. Prog. Brain Res. 1998; 118:3–11. [PubMed: 9932430]
18. Lander HM, Milbank AJ, Tauras JM, Hajjar DP, Hempstead BL, Schwartz GD, Kraemer RT, Mirza UA, Chait BT, Burk SC, Quilliam LA. Redox regulation of cell signalling. Nature. 1996; 381:380–381. [PubMed: 8632794]
19. Lander HM, Ogiste JS, Pearce SFA, Levi R, Novogrodsky A. Nitric Oxide-Stimulated Guanine-Nucleotide Exchange on P21(Ras). J. Biol. Chem. 1995; 270:7017–7020. [PubMed: 7706235]
20. Lander HM, Sehajpal PK, Novogrodsky A. Nitric-Oxide Signaling - a Possible Role for G-Proteins. J. Immunol. 1993; 151:7182–7187. [PubMed: 8258718]
21. Saavedra AP, Tsygankova OM, Prendergast GV, Dworet JH, Cheng G, Meinkoth JL. Role of cAMP, PKA and Rap1A in thyroid follicular cell survival. Oncogene. 2002; 21:778–788. [PubMed: 11850806]
22. Mittar D, Sehajpal PK, Lander HM. Nitric oxide activates Rap1 and Ral in a Ras-independent manner. Biochem. Biophys. Res. Commun. 2004; 322:203–209. [PubMed: 15313192]
23. Radi R, Beckman JS, Bush KM, Freeman BA. Peroxynitrite Oxidation of Sulfhydryls - the Cytotoxic Potential of Superoxide and Nitric-Oxide. J. Biol. Chem. 1991; 266:4244–4250. [PubMed: 1847917]
24. Koppenol WH, Moreno JJ, Pryor WA, Ischiropoulos H, Beckman JS. Peroxynitrite, a Cloaked Oxidant Formed by Nitric-Oxide and Superoxide. Chem. Res. Toxicol. 1992; 5:834–842. [PubMed: 1336991]
25. Beckmann JS, Ye YZ, Anderson PG, Chen J, Accavitti MA, Tarpey MM, White CR, Beckman JS. Extensive Nitration of Protein Tyrosines in Human Atherosclerosis Detected by Immunohistochemistry. Biol. Chem. Hoppe-Seyler. 1994; 375:81–88. [PubMed: 8192861]
26. Royall JA, Kooy NW, Beckman JS. Nitric oxide-related oxidants in acute lung injury. New Horiz. 1995; 3:113–122. [PubMed: 7704592]
27. Beckman JS, Beckman TW, Chen J, Marshall PA, Freeman BA. Apparent Hydroxyl Radical Production by Peroxynitrite - Implications for Endothelial Injury from Nitric-Oxide and Superoxide. Proc. Natl. Acad. Sci. USA. 1990; 87:1620–1624. [PubMed: 2154753]
28. Moreno JJ, Pryor WA. Inactivation of Alpha-1-Proteinase Inhibitor by Peroxynitrite. Chem. Res. Toxicol. 1992; 5:425–431. [PubMed: 1504267]
29. Silliams JG, Pappu K, Campbell SL. Structural and biochemical studies of p21Ras S-nitrosylation and nitric oxide-mediated guanine nucleotide exchange. Proc. Natl. Acad. Sci. USA. 2003; 100:6376–6381. [PubMed: 12740440]
30. Wittinghofer F, Krengel U, John J, Kabsch W, Pai EF. 3-Dimensional Structure of P21 in the Active Conformation and Analysis of an Oncogenic Mutant. Environ. Health Perspect. 1991; 93:11–15. [PubMed: 1773783]
31. Brunger AT, Milburn MV, Tong L, Devos AM, Jancarik J, Yamaizumi Z, Nishimura S, Ohtsuka E, Kim SH. Crystal-Structure of an Active Form of Ras Protein, a Complex of a Gtp Analog and the Hras P21 Catalytic Domain. Proc. Natl. Acad. Sci. USA. 1990; 87:4849–4853. [PubMed: 2191303]
32. Lander HM, Hajjar DP, Hempstead BL, Mirza UA, Chait BT, Campbell S, Quilliam LA. A molecular redox switch on p21(ras) - Structural basis for the nitric oxide-p21(ras) interaction. J. Biol. Chem. 1997; 272:4323–4326. [PubMed: 9020151]

33. Finkel T. Redox-dependent signal transduction. FEBS Letters. 2000; 476:52–54. [PubMed: 10878249]
34. Hancock JF. Ras proteins: Different signals from different locations. Nat. Rev. Mol. Cell Biol. 2003; 4:373–384. [PubMed: 12728271]
35. Rocks O, Peyker A, Kahms M, Verveer PJ, Koerner C, Lumbierres M, Kuhlmann J, Waldmann H, Wittinghofer A, Bastiaens PIH. An acylation cycle regulates localization and activity of palmitoylated Ras isoforms. Science. 2005; 307:1746–1752. [PubMed: 15705808]
36. Willumsen BM, Cox AD, Solski PA, Der CJ, Buss JE. Novel determinants of H-Ras plasma membrane localization and transformation. Oncogene. 1996; 13:1901–1909. [PubMed: 8934536]
37. Kuster GM, Pimentel DR, Adachi T, Ido Y, Brenner DA, Cohen RA, Liao R, Siwik DA, Colucci WS. alpha-adrenergic receptor-stimulated hypertrophy in adult rat ventricular myocytes is mediated via thioredoxin-1-sensitive oxidative modification of thiols on Ras. Circulation. 2005; 111:1192–1198. [PubMed: 15723974]
38. Teng KK, Esposito DK, Schwartz GD, Lander HM, Hempstead BL. Activation of c-Ha-Ras by nitric oxide modulates survival responsiveness in neuronal PC12 cells. J. Biol. Chem. 1999; 274:37315–37320. [PubMed: 10601298]
39. Mott HR, Carpenter JW, Campbell SL. Structural and functional analysis of a mutant Ras protein that is insensitive to nitric oxide activation. Biochemistry. 1997; 36:3640–3644. [PubMed: 9132016]
40. Williams JG, Pappu K, Campbell SL. Structural and biochemical studies of p21Ras S-nitrosylation and nitric oxide-mediated guanine nucleotide exchange. Proc. Natl. Acad. Sci. USA. 2003; 100:6376–6381. [PubMed: 12740440]
41. Thapar R, Williams JG, Campbell SL. NMR characterization of full-length farnesylated and non-farnesylated H-Ras and its implications for Raf activation. J. Mol. Biol. 2004; 343:1391–1408. [PubMed: 15491620]
42. Fenn JB, Mann M, Meng CK, Wong SF, Whitehouse CM. Electrospray Ionization for Mass-Spectrometry of Large Biomolecules. Science. 1989; 246:64–71. [PubMed: 2675315]
43. Karas M, Hillenkamp F. Laser Desorption Ionization of Proteins with Molecular Masses Exceeding 10000 Daltons. Anal. Chem. 1988; 60:2299–2301. [PubMed: 3239801]
44. Hillenkamp F, Karas M, Beavis RC, Chait BT. Matrix-Assisted Laser Desorption Ionization Mass-Spectrometry of Biopolymers. Anal. Chem. 1991; 63:A1193–A1202.
45. Horn DM, Zubarev RA, McLafferty FW. Automated de novo sequencing of proteins by tandem high-resolution mass spectrometry. Proc. Natl. Acad. Sci. USA. 2000; 97:10313–10317. [PubMed: 10984529]
46. Sannes-Lowery KA, Griffey RH, Kruppa GH, Speir JP, Hofstadler SA. Multipole storage assisted dissociation, a novel in-source dissociation technique for electrospray ionization generated ions. Rapid Commun. Mass Spectrom. 1998; 12:1957–1961. [PubMed: 9842743]
47. Sannes-Lowery KA, Hofstadler SA. Characterization of multipole storage assisted dissociation: Implications for electrospray ionization mass spectrometry characterization of biomolecules. J. Am. Mass Spectrom. 2000; 11:1–9.
48. Little DP, Speir JP, Senko MW, Oconnor PB, Mclafferty FW. Infrared Multiphoton Dissociation of Large Multiply-Charged Ions for Biomolecule Sequencing. Anal Chem. 1994; 66:2809–2815. [PubMed: 7526742]
49. Gauthier JW, Trautman TR, Jacobson DB. Sustained Off-Resonance Irradiation for Collision-Activated Dissociation Involving Fourier-Transform Mass-Spectrometry - Collision-Activated Dissociation Technique That Emulates Infrared Multiphoton Dissociation. Anal. Chim. Acta. 1991; 246:211–225.
50. Mirgorodskaya E, O'Connor PB, Costello CE. A general method for precalculation of parameters for sustained off resonance irradiation/collision-induced dissociation. J. Am. Soc. Mass Spectrom. 2002; 13:318–324. [PubMed: 11951969]
51. Zubarev RA, Kelleher NL, McLafferty FW. Electron capture dissociation of multiply charged protein cations. A nonergodic process. J. Am. Chem. Soc. 1998; 120:3265–3266.

52. Zubarev RA, Kruger NA, Fridriksson EK, Lewis MA, Horn DM, Carpenter BK, McLafferty FW. Electron capture dissociation of gaseous multiply-charged proteins is favored at disulfide bonds and other sites of high hydrogen atom affinity. J. Am. Chem. Soc. 1999; 121:2857–2862.
53. Leymarie N, Costello CE, O'Connor PB. Electron capture dissociation initiates a free radical reaction cascade. J. Am. Chem. Soc. 2003; 125:8949–8958. [PubMed: 12862492]
54. Kelleher RL, Zubarev RA, Bush K, Furie B, Furie BC, McLafferty FW, Walsh CT. Localization of labile posttranslational modifications by electron capture dissociation: The case of gamma-carboxyglutamic acid. Anal. Chem. 1999; 71:4250–4253. [PubMed: 10517147]
55. Stensballe A, Jensen ON, Olsen JV, Haselmann KF, Zubarev RA. Electron capture dissociation of singly and multiply phosphorylated peptides. Rapid Commun. Mass Spectrom. 2000; 14:1793–1800. [PubMed: 11006587]
56. Shi SDH, Hemling ME, Carr SA, Horn DM, Lindh I, McLafferty FW. Phosphopeptide/phosphoprotein mapping by electron capture dissociation mass spectrometry. Anal. Chem. 2001; 73:19–22. [PubMed: 11195502]
57. Mirgorodskaya E, Roepstorff P, Zubarev RA. Localization of O-glycosylation sites in peptides by electron capture dissociation in a fourier transform mass spectrometer. Anal. Chem. 1999; 71:4431–4436. [PubMed: 10546526]
58. O'Connor PB, Pittman JL, Thomson BA, Budnik BA, Cournoyer JC, Jebanathirajah J, Lin C, Moyer S, Zhao C. A new hybrid electrospray Fourier transform mass spectrometer: Design and performance characteristics. Rapid Commun. Mass Spectrom. 2006; 20:259–266. [PubMed: 16353130]
59. Jebanathirajah JA, Pittman JL, Thomson BA, Budnik BA, Kaur P, Rape M, Kirschner M, Costello CE, O'Connor PB. Characterization of a new qQq-FTICR mass spectrometer for post-translational modification analysis and top-down tandem mass Spectrometry of whole proteins. J. Am. Mass Spectrom. 2005; 16:1985–1999.
60. Kelleher NL, Lin HY, Valaskovic GA, Aaserud DJ, Fridriksson EK, McLafferty FW. Top down versus bottom up protein characterization by tandem high-resolution mass spectrometry. J Am Chem Soc. 1999; 121:806–812.
61. Mclafferty FW. High-Resolution Tandem Ft Mass-Spectrometry above 10-Kda. Acc. Chem. Res. 1994; 27:379–386.
62. Loboda A, Krutchinsky A, Loboda O, McNabb J, Spicer V, Ens W, Standing KG. Novel linac II electrode geometry for creating an axial field in a multipole ion guide. Eur. J. Mass Spectrom. 2000; 6:531–536.
63. Wilcox BE, Hendrickson CL, Marshall AG. Improved ion extraction from a linear octopole ion trap: SIMION analysis and experimental demonstration. J. Am. Mass Spectrom. 2002; 13:1304–1312.
64. Senko MW, Speir JP, Mclafferty FW. Collisional Activation of Large Multiply-Charged Ions Using Fourier-Transform Mass-Spectrometry. Anal. Chem. 1994; 66:2801–2808. [PubMed: 7978294]
65. Tsybin YO, Hakansson P, Budnik BA, Haselmann KF, Kjeldsen F, Gorshkov M, Zubarev RA. Improved low-energy electron injection systems for high rate electron capture dissociation in Fourier transform ion cyclotron resonance mass spectrometry. Rapid Commun. Mass Spectrom. 2001; 15:1849–1854. [PubMed: 11565103]
66. Kaur P, O'Connor PB. Algorithms for automatic interpretation of high resolution mass spectra. J. Am. Soc. Mass Spectrom. 2006; 17:459–468. [PubMed: 16464606]
67. Xu GZ, Kiselar J, He O, Chance MR. Secondary reactions and strategies to improve quantitative protein footprinting. Anal. Chem. 2005; 77:3029–3037. [PubMed: 15889890]
68. Xu GZ, Chance MR. Radiolytic modification of sulfur-containing amino acid residues in model peptides: Fundamental studies for protein footprinting. Anal. Chem. 2005; 77:2437–2449. [PubMed: 15828779]
69. Xu GZ, Chance MR. Radiolytic modification and reactivity of amino acid residues serving as structural probes for protein footprinting. Anal. Chem. 2005; 77:4549–4555. [PubMed: 16013872]

70. Galeva NA, Esch SW, Williams TD, Markille LM, Squier TC. Rapid method for quantifying the extent of methionine oxidation in intact calmodulin. J. Am. Soc. Mass Spectrom. 2005; 16:1470–1480. [PubMed: 16023363]

71. Guan ZQ, Yates NA, Bakhtiar R. Detection and characterization of methionine oxidation in peptides by collision-induced dissociation and electron capture dissociation. J. Am. Soc. Mass Spectrom. 2003; 14:605–613. [PubMed: 12781462]

72. Takamoto K, Chance MR. Radiolytic protein footprinting with mass spectrometry to probe the structure of macromolecular complexes. Annu. Rev. Biophys. Biomol. Struct. 2006; 35:251–275. [PubMed: 16689636]

73. Mirza UA, Chait BT, Lander HM. Monitoring Reactions of Nitric-Oxide with Peptides and Proteins by Electrospray-Ionization Mass-Spectrometry. J. Biol. Chem. 1995; 270:17185–17188. [PubMed: 7615515]

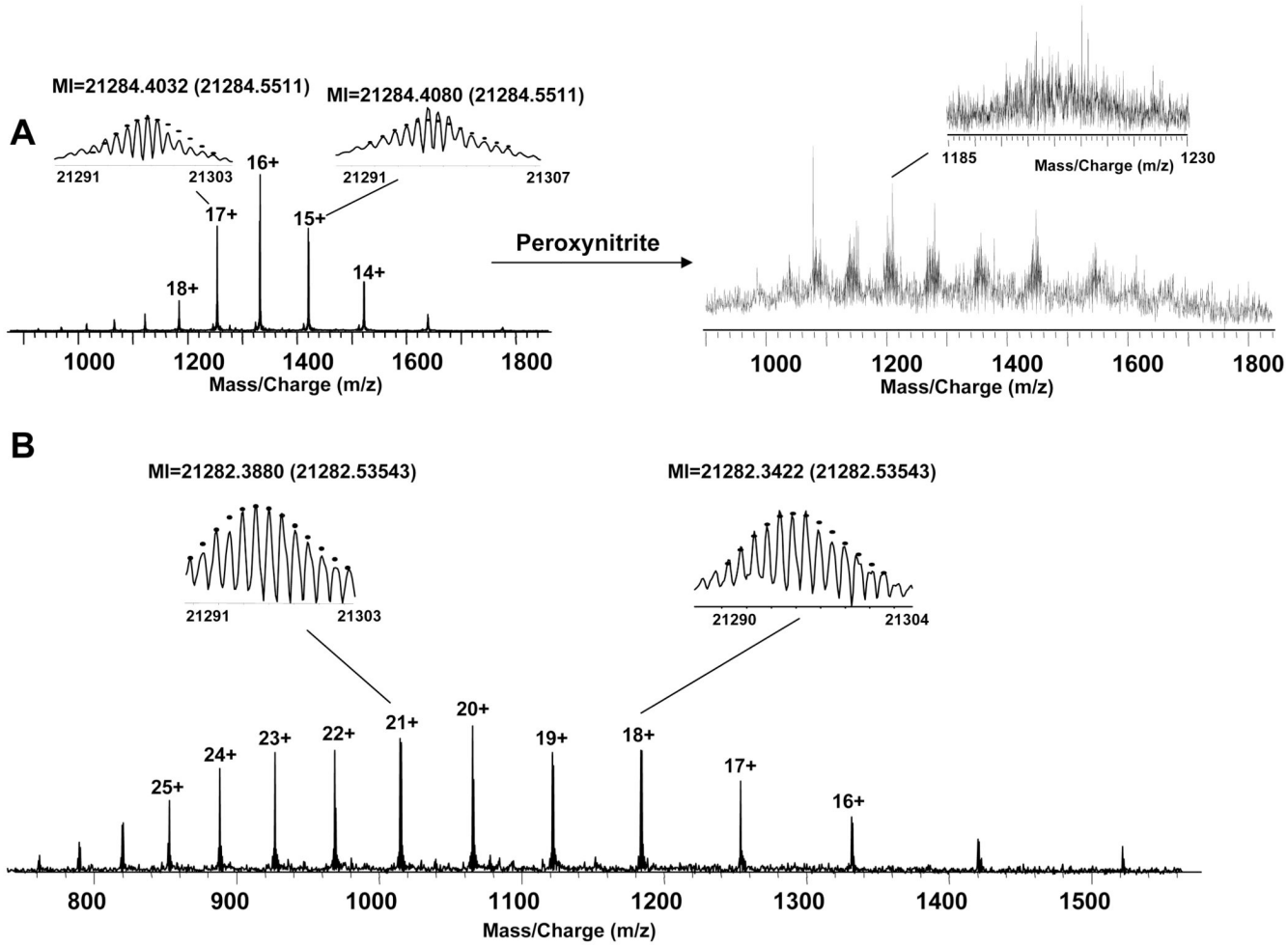

Figure 1.

A. (left) ESI spectrum of purified unmodified p21ras treated with DTT. (right) ESI spectrum of purified p21ras treated with peroxynitrite. Inset shows *m/z* 1185 – 1230. B. ESI spectrum of purified unmodified p21ras that is not treated with DTT.

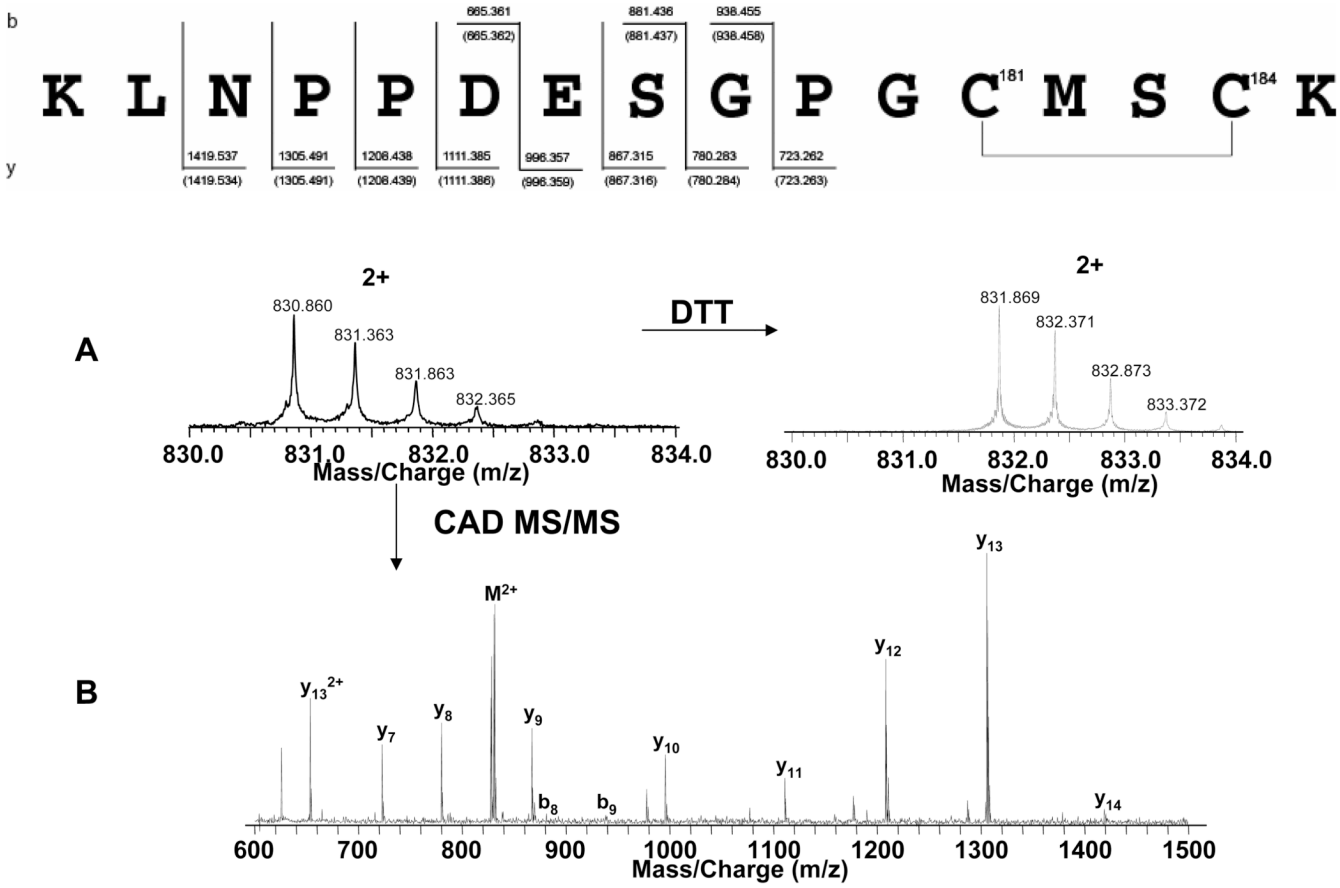

Figure 2.

A. (left) ESI spectrum of peptide 170–185 including the Cys181 – Cys184 disulfide bond (2+). (right) ESI spectrum of this peptide (2+) after DTT treatment. B. CAD MS/MS spectrum of this peptide. Top shows observed cleavages with measured masses and predicted masses in parentheses.

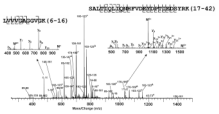

Figure 3.

Spectrum of p21ras treated with peroxynitrite and digested with trypsin. The major peaks are labeled with peptide positions. Those labeled with 002A indicate Met-O_x, those labeled with $^{\Delta}$ indicate both Met-O_s and Cys-SO_3H, and those labeled with $^{\circ}$ indicate Tyr-NO_2. Insets are the CAD MS/MS spectra of the unmodified peptides 6–16 and 17–42, which were used for internal *m/z* calibration.

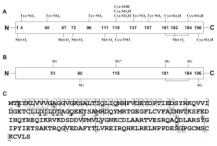

Figure 4.

A. Map of oxidative post-translational modifications detected on peroxynitrite-treated p21ras. B: Detected modifications on glutathiolated- p21ras. The most abundant glutathiolation on C118 confirmed by top-down analysis is labeled with *. C: Top down map of the major singly glutathiolated p21ras. The cleavages labeled with & include C118 glutathiolation.

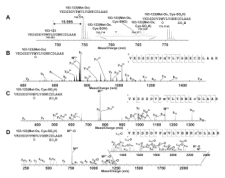

Figure 5.

A. *m/z* 745–775 from Figure 1B. T^* = trypsin autodigestion B. CAD MS/MS spectrum from peptide 103–123 with Met^{111}-O_x. C. CAD MS/MS spectrum from peptide 103–123 with both Met^{111}-O_x and Cys^{118}-SO_3H modifications. D. ECD MS/MS spectrum from peptide 103–123 with both Met^{111}-O_x and Cys^{118}-SO_3H modifications. Peptide sequences (right) show the observed cleavages.

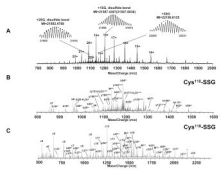

Figure 6.
Top down spectra of p21ras. A. ESI spectrum of purified glutathiolated p21ras. B. CAD MS/MS spectrum and C. ECD MS/MS spectrum on isolated +19 singly glutathiolated p21ras. The peak labeled with * indicates electronic noise.

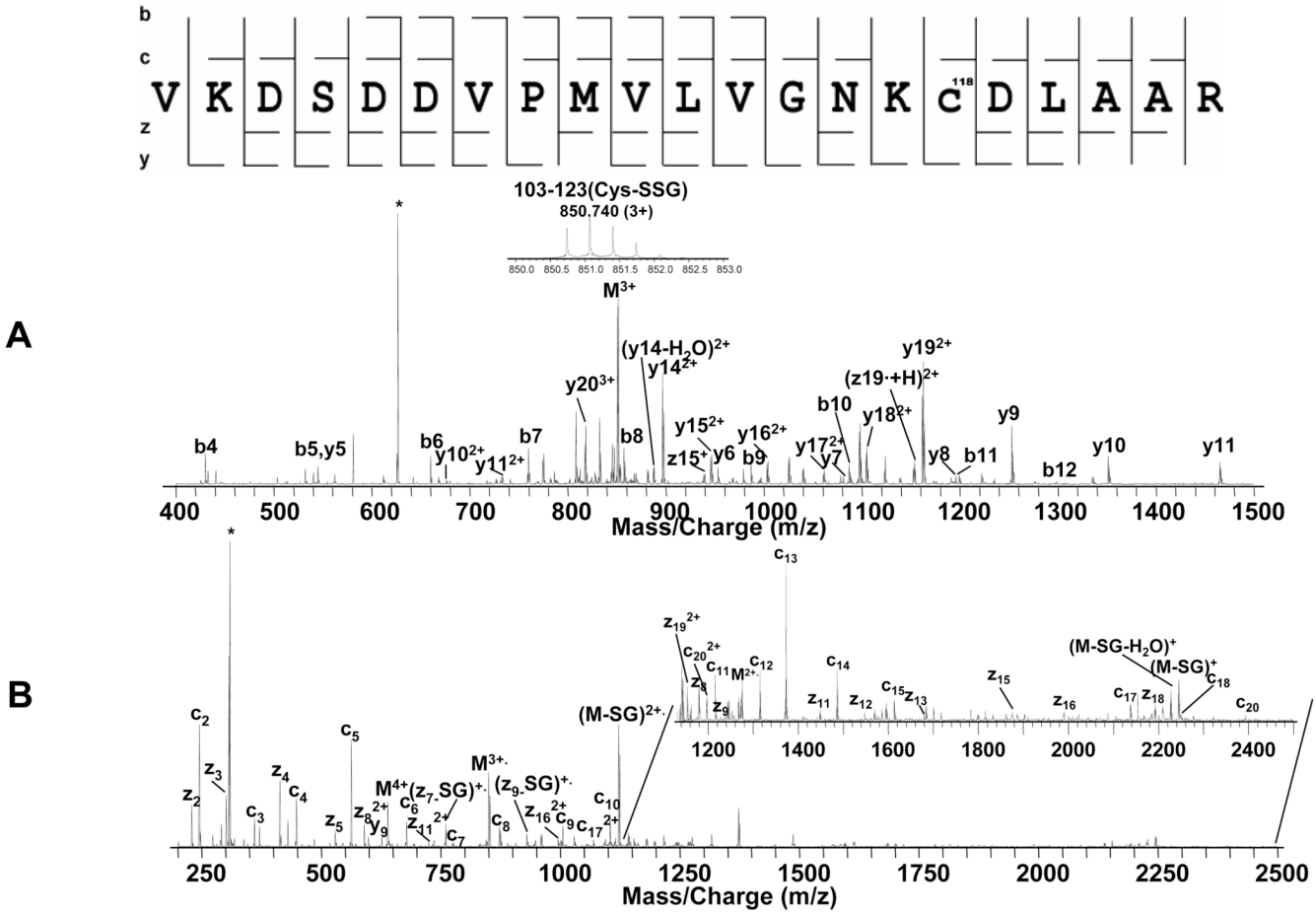

Figure 7.

A. CAD MS/MS spectrum of peptide 103–123 with Cys^{118}-SSG modification. The inset is the ESI spectrum of the precursor ion. B. ECD MS/MS spectrum of this modified peptide. The peak labeled with * indicates electronic noise. The sequence at the top shows the observed cleavages.

Table 1

Peak list of peroxynitrite-treated p21ras tryptic digest.

Position	Exp. Peak (in.)	Charge State	M+H(In.)	Theo. Mass	Error(ppm)
1–16(1Met-Ox)	541.9650	3	1623.8794	1623.8780	−0.83
1–16(1Met-Ox)	812.4440	2	1623.8802	1623.8780	−1.34
1–16(1Met-Ox,1Nit)	834.9350	2	1668.8622	1668.8631	0.55
6–16	478.3010	2	955.5942	955.5940	−0.18
6–16	955.5930	1	955.5930	955.5940	1.05
17–41	990.1520	3	2968.4404	2968.4406	0.07
17–42	774.6400	4	3095.5365	3095.5326	−1.27
17–42	1032.5170	3	3095.5354	3095.5326	−0.89
17–42(1Nit)	1047.5090	3	3140.5114	3140.5176	1.99
43–73(2Met-Ox)	899.4150	4	3594.6365	3594.6402	1.02
74–88	538.6060	3	1613.8024	1613.7998	−1.58
74–88	807.4040	2	1613.8002	1613.7998	−0.23
74–102	1148.5759	3	3443.7121	3443.7170	1.44
89–97	597.7820	2	1194.5562	1194.5544	−1.49
89–101	564.9510	3	1692.8374	1692.8346	−1.62
89–102	462.9900	4	1848.9365	1848.9357	−0.45
89–102	616.9830	3	1848.9334	1848.9357	1.27
89–102	924.9720	2	1848.9362	1848.9357	−0.26
89–102(1Nit)	631.9800	3	1893.9244	1893.9207	−1.93
102–123(1Met-Ox)	806.4150	3	2417.2294	2417.2281	−0.52
102–123(Met-Ox,1CysO3)	822.4110	3	2465.2174	2465.2128	−1.85
103–117(1Met-Ox)	544.6170	3	1631.8354	1631.8314	−2.42
103–123	749.0510	3	2245.1374	2245.1321	−2.34
103–123	1123.0700	2	2245.1322	2245.1321	−0.03
103–123(1Met-Ox)	566.0380	4	2261.1285	2261.1270	−0.67
103–123(1Met-Ox)	754.3790	3	2261.1214	2261.1270	2.50
103–123(1Met-Ox)	1131.0670	2	2261.1262	2261.1270	0.36
103–123(1Met-Ox,1CysO)	759.7140	3	2277.1264	2277.1219	−1.95
103–123(Met-Ox, 1Cys(NO))	764.3770	3	2291.1154	2291.1200	2.02

Position	Exp. Peak (in.)	Charge State	M+H(In.)	Theo. Mass	Error(ppm)
103–123(1Met-Ox,1cysO2)	765.0450	3	2293.1194	2293.1168	−1.11
103–123(1Met-Ox,1cysO3)	578.0340	4	2309.1125	2309.1117	−0.36
103–123(1Met-Ox,1cysO3)	770.3745	3	2309.1079	2309.1117	1.67
103–123(1Met-Ox,1cysO3)	1155.0620	2	2309.1162	2309.1117	−1.94
103–117(1Met-Ox)	816.4200	2	1631.8322	1631.8314	−0.47
103–128(1Met-Ox)	709.1110	4	2833.4205	2833.4188	−0.61
103–128(1Met-Ox)	945.1450	3	2833.4194	2833.4188	−0.19
105–123	673.3270	3	2017.9654	2017.9687	1.66
105–123(1Met-Ox)	678.6610	3	2033.9674	2033.9636	−1.84
105–123(1Met-Ox)	1017.4840	2	2033.9602	2033.9636	1.68
129–135	401.2150	2	801.4222	801.4219	−0.34
129–135	801.4230	1	801.4230	801.4219	−1.37
136–147	664.8410	2	1328.6742	1328.6738	−0.28
136–147(1Nit)	687.3350	2	1373.6622	1373.6589	−2.38
148–161	552.2905	3	1654.8559	1654.8553	−0.33
148–161	827.9320	2	1654.8562	1654.8553	−0.53
148–161(1Nit)	850.4240	2	1699.8402	1699.8404	0.13
150–161	466.5740	3	1397.7064	1397.7065	0.11
150–161	699.3560	2	1397.7042	1397.7065	1.66
150–161	1397.7030	1	1397.7030	1397.7065	2.50
150–161(1Nit)	721.8510	2	1442.6942	1442.6916	−1.78
162–169	540.3260	2	1079.6442	1079.6438	−0.35
170–185(1Met-Ox)	560.2475	3	1678.7269	1678.7239	−1.76
170–185(1Met-Ox)	839.8670	2	1678.7262	1678.7239	−1.36
170–189	688.9800	3	2064.9244	2064.9227	−0.80
170–189(1Met-Ox)	694.3110	3	2080.9174	2080.9176	0.12
170–189(1Met-Ox)	1040.9630	2	2080.9182	2080.9176	−0.28
170–189(1Met-Ox,1CysO3)	710.3070	3	2128.9054	2128.9023	−1.43
170–189(1Met-Ox,1CysO3)	1064.9570	2	2128.9062	2128.9023	−1.82
170–189(1Met-Ox,2CysO3)	1088.9490	2	2176.8902	2176.8870	−1.46
170–189(1Met-Ox,3CysO3)	1112.9400	2	2224.8722	2224.8717	−0.21

Position	Exp. Peak (in.)	Charge State	M+H(In.)	Theo. Mass	Error(ppm)
171–185(1Met-Ox)	775.8190	2	1550.6302	1550.6289	−0.82
171–189(1Met-Ox)	976.9160	2	1952.8242	1952.8226	−0.81
171–189(1Met-Ox,1CysO3)	1000.9070	2	2000.8062	2000.8073	0.56

Error Average =1.09 σ = 0.74